



# 1 **EcoDes-DK15: High-resolution ecological descriptors of vegetation** 2 **and terrain derived from Denmark's national airborne laser scanning** 3 **data set**

4 Jakob J. Assmann<sup>1</sup>, Jesper E. Moeslund<sup>2</sup>, Urs A. Treier<sup>1,3</sup>, Signe Normand<sup>1,3</sup>

5 <sup>1</sup>Department of Biology - Ecoinformatics and Biodiversity, Aarhus University, Aarhus, 8000, Denmark

6 <sup>2</sup>Department of Bioscience - Biodiversity, Aarhus University, Rønde, 8410, Denmark

7 <sup>3</sup>Department of Biology - Center for Sustainable Landscapes Under Global Change, Aarhus University, Aarhus, 8000,  
8 Denmark

9  
10 *Correspondence to:* Jakob J. Assmann ([j.assmann@bio.au.dk](mailto:j.assmann@bio.au.dk))

## 11 **Abstract**

12 Biodiversity studies could strongly benefit from three-dimensional data on ecosystem structure derived from contemporary  
13 remote sensing technologies, such as Light Detection and Ranging (LiDAR). Despite the increasing availability of such data  
14 at regional and national scales, the average ecologist has been limited in accessing them due to high requirements on computing  
15 power and remote-sensing knowledge. We processed Denmark's publicly available national Airborne Laser Scanning (ALS)  
16 data set acquired in 2014/15 together with the accompanying elevation model to compute 70 rasterized descriptors of interest  
17 for ecological studies. With a grain size of 10 m, these data products provide a snapshot of high-resolution measures including  
18 vegetation height, structure and density, as well as topographic descriptors including elevation, aspect, slope and wetness  
19 across more than forty thousand square kilometres covering almost all of Denmark's terrestrial surface. The resulting data set  
20 is comparatively small (~87 GB, compressed 16.4 GB) and the raster data can be readily integrated into analytical workflows  
21 in software familiar to many ecologists (GIS software, R, Python). Source code and documentation for the processing workflow  
22 are openly available via a code repository, allowing for transfer to other ALS data sets, as well as modification or re-calculation  
23 of future instances of Denmark's national ALS data set. We hope that our high-resolution ecological vegetation and terrain  
24 descriptors (EcoDes-DK15) will serve as an inspiration for the publication of further such data sets covering other countries  
25 and regions and that our rasterized data set will provide a baseline of the ecosystem structure for current and future studies of  
26 biodiversity, within Denmark and beyond.



## 27 **1 Introduction**

28 Over the last decades, airborne laser scanning (ALS) has become an established data source for providing fine-resolution  
29 measures of terrain and vegetation structure in ecological research (Moeslund et al., 2019; Guo et al., 2017; Zellweger et al.,  
30 2016). Despite its informative potential and the increasing number of openly available ALS data sets with regional and national  
31 extents (Vo et al., 2016), the uptake of these data sets for large-scale ecological research and applications (such as monitoring  
32 and conservation) has remained comparatively low (Bakx et al., 2019). The low uptake is likely a consequence of the  
33 considerable challenges that remain in handling these very large data sets, which require specialist expertise and software, as  
34 well as substantial amounts of data storage and processing power (Meijer et al., 2020; Vo et al., 2016; Pfeifer et al., 2014).  
35 Here, we address this issue for Denmark by providing a compact set of ecologically relevant measures of terrain characteristics  
36 and vegetation structure derived as raster outputs from the country's national ALS data set with a grain size of 10 m x 10 m.

37 The typical output from an ALS survey is a so-called point cloud that describes the physical structure of the surveyed area in  
38 three-dimensional space (Bakx et al., 2019; Vierling et al., 2008). In brief, short laser pulses are sent out from a Light Detection  
39 and Ranging (LiDAR) sensor mounted on an airplane (or drone) and reflected by surfaces such as bare ground, plants or  
40 buildings. The return timing of the reflected signal is measured and - with the help of information on the sensor's orientation  
41 and position - the precise location of the reflecting surface is determined in geographic space (Vierling et al., 2008). Depending  
42 on the properties of the LiDAR sensor, different surfaces will reflect the light with different strengths, allowing, for example,  
43 to separate returns from vegetation from those of bare ground (Vo et al., 2016; Wagner et al., 2006). Some surfaces may scatter  
44 large parts of the light which may result in multiple returns of different strengths, vegetation is amongst those (Wagner et al.,  
45 2006). Often, the raw signal is processed by the survey provider and the resulting data is delivered to the end user in the form  
46 of a point cloud of discrete returns, where each point is associated with information on geographic location, return strength  
47 (amplitude), acquisition timing etc. (Vo et al., 2016). For ALS data sets with large extents - such as Denmark's nationwide  
48 data set "DHM/Punktsky" - outputs from many survey flights are co-registered and merged, resulting in very large point clouds  
49 with hundreds of billions of points and data volumes of multiple Terabytes (Geodatastyrelsen, 2015). For further information  
50 on ALS methodology, we recommend Vo et al. (2016), Vierling et al. (2008) and Wagner et al. (2006).

51 Due to the ability to separate between ground and vegetation points, descriptors of terrain and vegetation structure can be  
52 derived from ALS point clouds. While early applications for ALS were focussed on generating simple digital elevation models  
53 (DEMs) for city and landscape planning, as well as canopy height estimates for commercial forestry (Bakx et al., 2019; Vo et  
54 al., 2016), recent advances in technology have allowed the calculation of more complex measures with wider applications.  
55 Terrain derived measures of ecological interests include topographic slope, aspect (i.e., slope direction), solar irradiation,  
56 wetness etc. (e.g., Moeslund et al., 2019; Zellweger et al., 2016; Ceballos et al., 2015), and vegetation structural descriptors  
57 include vegetation density, canopy height diversity, canopy roughness and many more (e.g., Bakx et al., 2019; Moeslund et  
58 al., 2019; Coops et al., 2016). It is important to note that sensor and point cloud characteristics may limit the type of measures



59 that can be meaningfully derived from ALS data (Bakx et al., 2019). This applies especially to the point cloud density, which  
60 needs to be high enough to meaningfully resolve the structure of understory layers in forest systems (Bakx et al., 2019) or  
61 ecosystems with vegetation of low stature such as grasslands or tundra (Boelman et al., 2016). Nonetheless, even simpler ALS  
62 derived descriptors of terrain and vegetation structure can be of high value for ecological applications, as fieldwork-derived  
63 alternatives are often too costly and difficult to collect over large extents (Vierling et al., 2008).

64 ALS data has provided critical information for research on biodiversity and habitat characteristics over the recent years, and  
65 its importance in ecological research is likely to increase in the future. Numerous biodiversity studies have successfully  
66 deployed ALS to study organisms like plants (Mao et al., 2018; Lopatin et al., 2016; Zellweger et al., 2016; Ceballos et al.,  
67 2015; Moeslund et al., 2013; Leutner et al., 2012), fungi (Peura et al., 2016; Thers et al., 2017), bryophytes, lichens (Moeslund  
68 et al., 2019), mammals (Tweedy et al., 2019; Froidevaux et al., 2016) and birds (see Bakx et al. (2019) for a comprehensive  
69 review) both in open landscapes and in forests. These studies have all emphasized the value of ALS for representing fine-scale  
70 (~ 10 m resolution) terrain or vegetation structural variation of importance to local biodiversity patterns. Furthermore,  
71 Valbuena et al. (2020) recently considered ALS data to be one of the key resources for deriving ecosystem morphological  
72 traits in the global assessment of Essential Biodiversity Variables (EBVs). Finding ways of making regional and nationwide  
73 ALS data more accessible to the average ecologist is therefore not only a critical priority for accelerating research on regional  
74 biodiversity patterns and species - habitat relationships, but also for the facilitation of global assessments such as those carried  
75 out by IPBES (2019) and alike.

76 To open up opportunities for researchers and practitioners not familiar with ALS processing or without access to the required  
77 facilities, we present a new national ALS based data set for Denmark primarily aimed at ecological research with possible uses  
78 in other disciplines. With a grain size of 10 m, these ecological descriptor (EcoDes) rasters provide a snapshot of high-  
79 resolution measures of vegetation height, structure and density, as well as topographic descriptors including elevation, aspect,  
80 slope and wetness for almost all of Denmark's terrestrial surface between spring 2014 and summer 2015 (DK15). In this  
81 publication, we a) describe the source data and outline the processing workflow (Sect. 2.1-2.3), b) summarise the data set's  
82 main characteristics (Sect. 3.1-3.2), c) describe each variable in detail and highlight its use and limitations (Sect. 3.3-3.4), d)  
83 provide guidance on data access and illustrate how the data could be used in an example of ecological landscape classification  
84 (Sect. 4). We finish by e) briefly discussing the general limitations of the data set and processing workflow, as well as providing  
85 perspectives on how the presented data can be complemented with other data sources (Sect. 5). We hope that ease of access  
86 and thorough documentation of the EcoDes-DK15 data set will encourage uptake and facilitate the development of future  
87 versions of similar data sets in Denmark and beyond.



## 88 2 Source data and processing workflow overview

### 89 2.1 Denmark - geography and ecology

90 Located in Northern Europe, Denmark (without Greenland and the Faroe Islands) has an approximate land area of 43 thousand  
91 square kilometres, comprising the large peninsula of Jutland and 443 named islands. The relatively flat (highest point is 171  
92 m above sea level) landscape predominantly consists of arable land and production forest with relatively small patches of  
93 natural or semi-natural areas such as heathlands, grasslands, fresh and salt meadows, bogs, dunes, lakes, streams and deciduous  
94 forests.

### 95 2.2 ALS and elevation source data

96 The Danish elevation model (DHM) is an openly available nationwide data set providing various products based on ALS data.  
97 Here, we used the DHM/Point-cloud (DHM/Punktsky), the classified georeferenced ALS point cloud product, and the  
98 DHM/Terrain (DHM/Terræn), the digital elevation model product, both based on data collected in 2014 and 2015 (Table 1,  
99 see Nord-Larsen et al., 2017 for details on acquisition time). The DHM data set is currently hosted and maintained by the  
100 Agency for Data Supply and Efficiency, Denmark (<https://sdfe.dk/>) and can be downloaded from <https://kortforsyningen.dk/>  
101 (see guidance on GitHub code repository). The DHM/Point-cloud product is a collection of 1 x 1 km tiles of three-dimensional  
102 point clouds with attributes such as position, intensity, point source ID, or classification. Point classification includes for  
103 example ground, vegetation, and buildings. The point density is on average 4-5 points per square meter with a horizontal and  
104 vertical accuracy of 0.15 and 0.05 metres, respectively. Additional information on the data set can be found in Geodatastyrelsen  
105 (Geodatastyrelsen, 2015 - in Danish), Thers et al. (2017) and Nord-Larsen et al (2017). The DHM/Point-cloud product is  
106 provided in a LAZ-format and in the ETR89 UTM 32N horizontal (EPSG: 25832) and DVR90 vertical reference system. The  
107 DHM/Terrain product is a rasterized digital model of the terrain height above sea level in 0.4 m resolution. This product is  
108 provided in a 32-bit GeoTiff format, using the same 1 km x 1 km tiling convention and spatial reference system as the  
109 DHM/Point-cloud.

110

111 **Table 1:** Overview of the key data sources used for generating the EcoDes-DK15 data set.

Data source	Year	Used for	Data provider	Available from
DHM/Pointcloud (DHM/Punktsky)	2014/15	Vegetation Descriptors	Danish Agency for Data Supply and Efficiency	<a href="https://download.kortforsyningen.dk">https://download.kortforsyningen.dk</a>
DHM/Terrain (DHM/Terræn)	2014/15	Terrain Descriptors	Danish Agency for Data Supply and Efficiency	<a href="https://download.kortforsyningen.dk">https://download.kortforsyningen.dk</a>

112

113 The DHM/Terrain 2014/2015 and DHM/Point-cloud data sets 2014/2015 do not fully overlap in the 1 km x 1 km tiles of  
114 Denmark covered. While both data sets contain matching tile pairs for 49835 tiles, 291 tiles do not have a matching partner



115 tile in one of the data set (209 DHM/Point-cloud tiles have no corresponding DHM/Terrain tile and 82 DHM/Terrain tiles have  
116 no corresponding DHM/Point-cloud tile). We removed these incomplete tile pairs from the data generation prior processing.

## 117 **2.3 Processing**

118 We processed the source data using OPALS 2.3.2.0 (Pfeifer et al., 2014), Python 2.7 (Van Rossum and Drake Jr, 1995), pandas  
119 0.24.2 (Reback et al., 2019), SAGA GIS 2.3.2 (Conrad et al., 2015) from OSGeo4W64 and GDAL 2.2.4 (GDAL/OGR  
120 contributors, 2018) also from OSgeo4W64. The large number of tiles and variables to be calculated, required us to develop a  
121 robust processing pipeline, which we realised as a set of Python modules. The source code is openly available via a GitHub  
122 code repository (see Sect. 6). Processing was carried out on a Dell PowerEdge R740xd computational server (Windows 2012  
123 R2 64-bit Operating System, 2x Intel Xeon Platinum 8180 Processors and 1.536TB RAM). The processing of the whole data  
124 set took approximately 45 days to complete.

125

### 126 **2.3.1 Processing workflow**

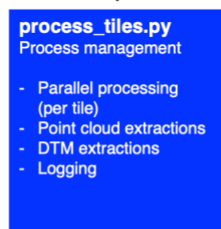
127 To facilitate the processing of the large data set, we first generated a set of compact Python modules providing a programming  
128 interface that allows for the calculation of the individual variables outlined in Sect. 3. The individual routines were then  
129 integrated into a Python script mediating the processing workflow in parallel, while carrying out error handling, logging and  
130 progress tracking. The schematic of the processing workflow and the Python modules is outlined in Fig. 1. Detailed information  
131 is available on the GitHub repository, including instructions on how to set up the processing, documentation on the functions  
132 provided by the Python modules, as well as detailed intext commentary of the code.



## Processing Workflow Overview

### Inputs

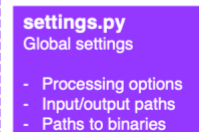
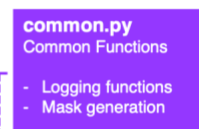
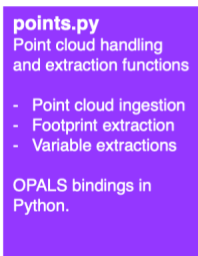
- Nationwide ALS point cloud  
~ 49k tiles
- Nationwide terrain model at 0.4 m res.  
~ 49k tiles



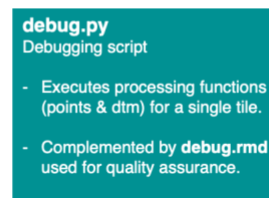
### Outputs

- Ecological variables, raster 10 m res.  
18 x terrain and cover structure descriptors  
~ 49k tiles each

### dk\_lidar Python Modules



### Helper scripts Independent python scripts



133

134 **Figure 1:** Diagram of the processing workflow, the *dk\_lidar* Python module and helper scripts. The workflow requires two  
 135 inputs: a pre-classified set of point cloud tiles and a paired set of digital terrain model (dtm) tiles. The process management is  
 136 handled by the *process\_tiles.py* script which facilitates processing of each tile pair (dtm and point cloud) in parallel and logs  
 137 the progress. For each tile, *process\_tiles.py* calls a specified set of extraction and processing functions from the *dk\_lidar*  
 138 modules. Point cloud extraction functions are specified in *points.py* and terrain model extraction functions are specified in  
 139 *dtm.py*. The *dk\_lidar* modules also contain two further files, *common.py* a script containing specifications of common functions  
 140 used by the *points.py* and *dtm.py*, as well as *settings.py* which is used to set global processing options, specify file paths etc.  
 141 Finally, two helper scripts are provided *progress\_monitor.py* which facilitates progress monitoring and estimates the time  
 142 remaining and *debug.py* a script for testing the workflow for a single tile. Together the Python scripts and modules allow to  
 143 generate the ecological descriptor outputs from the two input variables. Further documentation of the *dk\_lidar* modules and  
 144 workflow scripts can be found on the GitHub repository associated with this publication:  
 145 <https://github.com/jakobjassmann/ecodes-dk-lidar>.



### 146 3 Data set description and known limitations

#### 147 3.1 Extent, projection, resolution and data format

148 EcoDes-DK15 covers the majority of Denmark's land area, including the island of Bornholm (approximate extent: 54.56 °N  
149 to 57.75 °N, 8.07 °E to 15.20 °E). The data is projected in ETR89 UTM 32 N based on the GRS80 spheroid (EPSG: 25832).  
150 The data set is available as GeoTIFFs with 10 m grain size via a data repository on Zenodo (see Sect. 6). For each variable the  
151 nation-wide data are split into 49835 raster tiles of 1 km x 1 km with a 10 m grain size based on 25-fold aggregations of the  
152 0.4 m national grid of Denmark. A virtual raster mosaic (VRT) file is provided for each variable, and a file containing the tile  
153 footprint geometries can be used for geographical sub-setting of the data. We also provide masks for inland water and the sea.  
154

155 The final data set consists of just under 87 GB of data (compressed for download 16.4 GB). To reduce the size of the data set  
156 we converted numerical values from floating point precision to 16-bit integers where possible. In some cases, this required us  
157 to stretch the values by a set factor to maintain information content beyond the decimal point. The variable conversion factors  
158 are available as a csv file provided with the data set and in Table 2. Missing data is denoted by a value of -9999 throughout  
159 the data set (NODATA-value).

#### 160 3.2 Overview and file naming convention

161 An overview of the eighteen terrain and vegetation structure variables as well as the auxiliary data provided can be found in  
162 Table 2. Generally, the variable names in Table 2 reflect the prefix of the file name of a GeoTiff file within the data set. This  
163 prefix is followed by a suffix representing the unique identifier for each tile based on the UTM coordinates of the tile (see  
164 Sect. 3.4.3 for more detail). When working with the complete data set, tiles from the same variable are grouped within a folder  
165 using the same variable name as used for the file name prefix. For example, for the tile with the unique id “6239\_446” the  
166 GeoTiff for the “dtm\_10m” variable can be found in “dtm\_10m/dtm\_10m\_6239\_446.tif”. The exceptions are the point counts,  
167 vegetation proportions and point source information, please see the relevant sections below for more detail.  
168

169 **Table 2:** Brief overview of the eighteen main EcoDes-DK15 variables and variable groups, their ecological meaning, unit,  
170 format and conversion factor. In addition to the 70 raster layers for the main variables, the data set contains six layers of  
171 auxiliary information (see Sect. 3.7). Note: to obtain the correct unit, the variable value needs to be divided by the conversion  
172 factor.  
173

Variable(s)	Ecological meaning	Unit	Format	Conversion factor	Number of layers
dtm_10m	elevation	m	16-bit integer	100	1
aspect	topographic aspect	degrees	16-bit integer	10	1



slope	topographic slope	degrees	16-bit integer	10	1
heat_load_index	proxy of radiation and wetness	unitless	16-bit integer	10000	1
solar_radiation	solar radiation	ln(MJ x cm <sup>-2</sup> x yr <sup>-1</sup> )	16-bit integer	1000	1
openness_mean	topographic position	degrees	16-bit integer	1	1
openness_difference	presence of linear landscape features	degrees	16-bit integer	1	1
twi	topographic wetness	unitless	16-bit integer	1000	1
amplitude_mean	complex**	undefined	32-bit float	1	1
amplitude_sd	complex**	undefined	32-bit float	1	1
canopy_height	vegetation height	m	16-bit integer	100	1
normalized_z_mean	average structural height (incl. vegetation and buildings)	m	16-bit integer	100	1
normalized_z_sd	variation in structural height (incl. vegetation and buildings)	m	16-bit integer	100	1
point_counts*	number of returns in ground, water, building and vegetation point classes; total return count and vegetation return counts in height bins	count	16-bit integer	1	30
vegetation_proportion*	proportion of vegetation returns in height bins	proportion	16-bit integer	10000	24
vegetation_density	ratio of vegetation returns to total returns	proportion	16-bit integer	10000	1
canopy_openness	ratio of ground and water returns to total returns	proportion	16-bit integer	10000	1
building_proportion	ratio of building returns to total returns		16-bit integer	10000	1
point_source_info*	point source / flight strip information	varied, see description	varied, see description	varied, see description	4
masks	inland water and sea mask	binary	16-bit integer	1	2

174

175 \* Variable group containing multiple individual variables, see intext description for detail.

176 \*\* The amplitude variables are difficult to interpret, but can serve as useful indicators for vegetation classification and  
 177 biodiversity studies. Please see intext description for more detail.





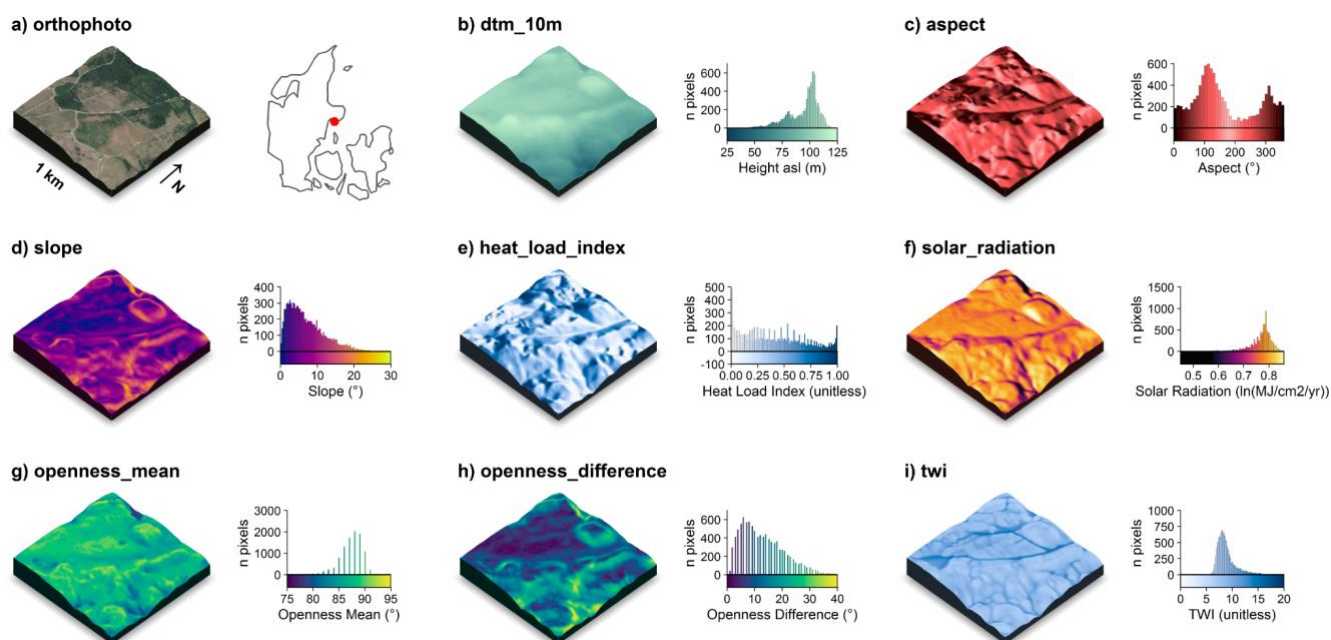
### 178 3.3 Completeness of the data set

179 The processing of the data set was almost completely successful. Processing failed on average for only 41 out of the 49835  
180 tiles per variable with a maximum of 83 tiles failing for the *canopy\_height*, *normalized\_z\_mean* and *normalized\_z\_sd* variables.  
181 The majority of these tiles were located on the fringes of the data set, including sand spits, sandbanks etc, we therefore did not  
182 attempt re-processing of those tiles. Instead, we generated nodata-value rasters for all missing variable - tile combinations (i.e.  
183 we assigned -9999 to all cells in those tiles). We provide a text file listing the affected “nodata” tiles in the folder of each  
184 variable (the file is named empty\_tiles\_XXX.txt, where XXX is the variable name).

### 185 3.4 Elevation-model derived variables

186 The following variables were solely derived from the 0.4 m digital elevation model (DHM/Terrain). Visualisations of these  
187 variables for an example tile in the Mols Bjerger area are shown in Fig. 2.

188



189

190 **Figure 2:** Illustration of the terrain model derived variables for a 1 km x 1 km tile in the Mols Bjerger area (tile id: 6230\_595).  
191 An orthophoto and the tile location relative to Denmark are shown in (a). The terrain model (dtm\_10m) is illustrated in (b).  
192 The terrain derived variables comprise of: c) the topographic aspect, d) the topographic slope, e) the heat load index following  
193 Kuehne et al. f) the estimated incident solar radiation, g) the landscape openness mean, h) the landscape openness difference  
194 in the eight cardinal directions and i) the topographic wetness index (TWI) based on Kopecký et al (2020). For visualisation  
195 purposes, we amplified the altitude above sea-level by a factor of two in the 3D visualisations. The 3D raster visualisations



196 were generated using the rayshader v0.19.2 package in R (Morgan-Wall, 2020). Orthophoto provided by the Danish Agency  
197 for Data Supply and Efficiency (<https://sdfe.dk/hent-data/fotos-og-geodanmark-data/>).

### 198 **3.4.1 Elevation (dtm\_10m)**

199 We aggregated the 0.4 m DEM by mean to match the 10 m x 10 m national grid of the remainder of the data set. We used  
200 *gdalwarp* to carry out the aggregations. Values represent the elevation above sea level in metres multiplied by a factor of 100,  
201 rounded to the nearest integer and converted to 16-bit integer.

### 202 **3.4.2 Aspect (aspect)**

203 The topographic aspect describes the orientation of a slope in the terrain and may, amongst other things, be related to plant  
204 growth through light and moisture availability. We calculated the aspect in degrees, with 0° indicating North, 90° East, 180°  
205 South and 270° West. Values represent the aspect derived from a 10 m aggregate of the elevation model (aggregated by mean  
206 with 32bit floating point precision). Calculations were carried out using *gdaldem* binaries and the “aspect” option, which by  
207 default uses Horn’s method to calculate the aspect (Horn, 1981). To avoid edge effects, all calculations were done on a mosaic  
208 that included the focal tile and all available directly neighbouring tiles (maximum eight). The mosaic was cropped back to the  
209 extent of the focal tile upon completion of the calculations. We then converted the value for each cell from radian to degrees,  
210 multiplied it by a factor of 10, rounded to the nearest integer and stored the results as a 16-bit integer. Finally, we assigned a  
211 value of -10 (-1°) to all cells where the slope was 0° (flat). Limitations in the aspect arise in relation to edge effects that occur  
212 where a neighbourhood mosaic is incomplete for a focal tile (i.e., less than eight neighbouring tiles), such as for tiles along the  
213 coastline or at the edge of the covered extent. For those tiles, no aspect can be derived for the rows or columns at the edge of  
214 the mosaic. The cells in those rows and columns have no neighbouring cells and were assigned the no data value (-9999).

### 215 **3.4.3 Slope (slope)**

216 The topographic slope describes the steepness of the terrain and amongst other things may be related to moisture availability,  
217 exposure and erosion. We derived the topographic slope in degrees with a 10 m grain size from a mean aggregate of the  
218 elevation model (32bit floating point precision) using the *gdaldem* binaries with the “slope” option, which by default use  
219 Horn’s method to calculate the slope (Horn, 1981). To avoid edge effects, we carried out the calculations on a mosaic including  
220 the focal tile and all available directly neighbouring tiles (maximum eight). The mosaic was cropped back to the extent of the  
221 focal tile upon completion of the calculations. The value for each cell was converted from radian to degrees, multiplied by a  
222 factor of 10, rounded to the nearest integer and stored as a 16-bit integer. Limitations in the slope arise in relation to edge  
223 effects that occur where a neighbourhood mosaic is incomplete for a focal tile (i.e., less than eight neighbouring tiles), such as  
224 for tiles along the coastline or at the edge of the covered extent. For those tiles, no slope can be derived for the rows or columns  
225 at the edge of the mosaic. These cells in those rows and columns have no neighbouring cells and *gdaldem* assigns the no data  
226 value (-9999) to these cells.



#### 227 **3.4.4 Landscape openness mean (openness\_mean)**

228 Landscape openness is a landform descriptor that indicates whether a cell is located in a depression or elevation of the  
229 landscape. We calculate the landscape openness following Yokoyama et al. (2002) using the OPALS implemented algorithms.  
230 We used a mean aggregate of the elevation model with 10 m grain size and 32bit floating point precision, and derived the  
231 mean landscape openness for a cell as the mean of the landscape openness in all eight cardinal directions with a search radius  
232 of 150 m. We chose to base this variable on the aggregated 10 m elevation model and a 150 m search radius, as we think that  
233 these are best suited to describe the landscape scale variation in the landforms of Denmark. The Danish landscapes are  
234 characterised by gently undulating terrain, valleys forged by small to medium sized rivers and dune systems along the  
235 coastlines. First, we generated a mosaic including the focal tile and all available tiles in the direct neighbourhood (max. eight  
236 neighbouring tiles) to reduce edge effects in subsequent calculations. The mean of the positive openness for all eight cardinal  
237 directions with search radius of 150 m was then derived for all cells in the mosaic using the OPALS Openness module (options:  
238 feature = 'positive', kernelSize = 15 and selMode = 0). Next, the mean openness per cell was converted from radians to degrees,  
239 rounded to the nearest integer and stored as a 16-bit integer. For incomplete neighbourhood mosaics (i.e. containing less than  
240 eight neighbouring tiles) we then masked out cells within the first 150 m of all edges where a neighbourhood tile was missing.  
241 Finally, the output was cropped back to the extent of the focal tile. As a consequence of the edge effect related masking, the  
242 focal tiles on the fringes of the data set, such as those on coastlines or at the edge of the coverage area, have no data available  
243 for the first 150 m. The corresponding cells for the affected areas are set to the NODATA value -9999.

#### 244 **3.4.5 Landscape openness difference (openness\_difference)**

245 In addition to the mean of the landscape openness, we also derived a landscape openness difference measure. This difference  
246 measure is an indicator of whether a cell is part of a linear feature in the landscape that runs in one cardinal direction, such as  
247 a ridge or valley, therefore providing additional information to the landscape openness\_mean variable. We calculated the  
248 landscape openness difference based on the 10 m mean aggregate of the elevation model (32bit floating point precision) and  
249 with a search radius of 50 m. We chose these parameters as we consider them best suited to capture the relatively narrow  
250 valleys and ridgetops common in the Danish landscape. First, we generated a mosaic including the focal tile and all available  
251 tiles in the direct neighbourhood (max. eight neighbouring tiles) to reduce edge effects in subsequent calculations. We then  
252 calculated the minimum and maximum of the positive landscape openness from all eight cardinal directions for all cells in the  
253 mosaic using the OPALS Openness module with a search radius of 50 m (feature = 'positive', kernelSize = 5, selMode = 1  
254 for minimum and selMode = 2 for maximum). Next, we converted the minimum and maximum values from radian to degrees  
255 and calculated the difference between the maximum and minimum value. We rounded the result to the nearest full degree. For  
256 the cases where the neighbourhood mosaic was incomplete, i.e., containing less than eight neighbouring tiles, we masked out  
257 all cells within the first 50 m of all edges with a missing neighbourhood tile. The final output mosaic was then cropped to the  
258 extent of the focal tile and stored as a 16-bit integer GeoTIFF. As a consequence of the edge effect related masking, focal tiles



259 on the edges of the data set, such as those on coastlines or at the edge of the coverage area, have no data available for the first  
260 50 m.

### 261 3.4.6 Solar Radiation (*solar\_radiation*)

262 Incident solar radiation is a key parameter for plant growth and indicator for local microclimate. We estimated the amount of  
263 incident solar radiation received per square centimetre per year from the slope and aspect computed as described above.  
264 Calculations were implemented using *gdal\_calc*, following equation 3 specified in McCune and Keon (2002):

265

$$\begin{aligned} solar\_radiation = & 0.339 + \\ & 0.808 \times \cos(L) \times \cos(S) - \\ & 0.196 \times \sin(L) \times \sin(S) - \\ & 0.482 \times \cos(180 - |(180 - A)|) \times \sin(S) \end{aligned} \quad (1)$$

266

267 where  $L$  is the centre latitude of the cell in degrees,  $S$  is the slope of the cell in degrees and  $A$  is the aspect of the cell in degrees.  
268 The resulting estimate is given in:  $\ln(\text{MJ} \times \text{cm}^{-2} \times \text{yr}^{-1})$  (McCune and Keon, 2002). Slope and aspect for each 10 m x 10 m grid  
269 cell were sourced from the slope and aspect rasters. We stretched the results by a factor of 1000, rounded to the nearest integer  
270 and stored them as 16-bit integers. Due to propagation from the calculation of slope variable, no solar radiation values can be  
271 calculated for cells found right on the edge of the data set, for example in tiles situated along the coastline or at the edge of the  
272 sampling extent.

### 273 3.4.7 Heat Load Index (*heat\_load\_index*)

274 The heat load index (McCune and Keon, 2002) was originally developed as an indicator for temperature based solely on aspect,  
275 but this characteristic is probably better captured in our solar radiation variable (see above) that was developed to improve  
276 shortcomings in the heat load index (McCune and Keon, 2002). However, in a previous study (Moeslund et al., 2019) we show  
277 that - in Denmark - the index was moderately correlated with soil moisture, and can therefore serve as an useful indicator of  
278 the amount of moisture available to plants. We calculated the heat load index based on the aspect rasters (described above)  
279 following the equation specified in McCune and Keon (2002) using *gdal\_calc*:

280

$$heat\_load\_index = \frac{(1 - \cos(A - 45))}{2} \quad (2)$$

281

282 where  $A$  is the aspect in degrees. We stretched the result by a factor of 10000, rounded to the nearest integer and stored it as a  
283 16-bit integer. As the *heat\_load\_index* is not meaningfully defined for flat cells (slope = 0° / aspect = -1°), we set the value of



284 those cells to no data (-9999). Finally, for cells that are located on the outermost edges of the data set the `heat_load_index` is  
285 not defined due to propagation of the nodata value assigned to the aspect in those cells.

### 286 **3.4.8 Topographic wetness index (twi)**

287 The Topographic wetness index (TWI) provides a proxy measure of soil moisture or wetness based on the hydrological flow  
288 modelled through a digital terrain model. Here, we derived the TWI following the method recommended by Kopecký et al.  
289 (2020). We based our calculations on the aggregated 10 m elevation model (`dtm_10m`, 16bit integer) and used a neighbourhood  
290 mosaic (max. 8 neighbours) for each focal tile to derive the TWI. The exact procedure is detailed in the next paragraph. As  
291 such the index values calculated by us only consider a catchment the size of one tile and all its neighbours (for non-edge tiles  
292 this is a 3 km x 3 km catchment, for edge tiles it is smaller depending on the completeness of the neighbourhood mosaic). We  
293 then cropped the resulting output back to the extent of the focal tile, stretched the TWI values by a factor of 1000, rounded to  
294 the next full integer and stored the results as a 16-bit integer.

295 We calculated the TWI using SAGA GIS v. 7.8.2 binaries. First, we sink-filled the neighbourhood mosaic of the terrain model  
296 using the `ta_preprocessor 5` module and the option “MINSLOPE 0.01” (Wang and Liu, 2006). Second, we calculated the flow  
297 accumulation based on the sink-filled neighbourhood mosaic of the terrain model (from step one) using the `ta_hydrology 0`  
298 module with options “METHOD 4” and “CONVERGENCE 1.0” (Freeman, 1991; Quinn et al., 1991). Third, we derived the  
299 flow width and specific catchment area based on the sink-filled neighbourhood mosaic of the terrain model (from step one)  
300 and the flow accumulation (from step two) using the module `ta_hydrology 19` (Gruber and Peckahm, 2008; Quinn et al., 1991).  
301 Fourth, we calculated the slope based on the sink-filled neighbourhood mosaic of the terrain model (from step one) using the  
302 `ta_morphometry 0` module with option “METHOD 7” (Haralick, 1983). Finally, we derived the TWI based on the specific  
303 catchment area (from step three) and slope (from step four) using the module `ta_hydrology 20` (Beven and Kirkby, 1979;  
304 Böhner and Selige, 2006; Moore et al., 1991). For detailed descriptions of the modules used, please refer to the SAGA GIS  
305 documentation (SAGA-GIS Tool Library Documentation v7.8.2, 2021).

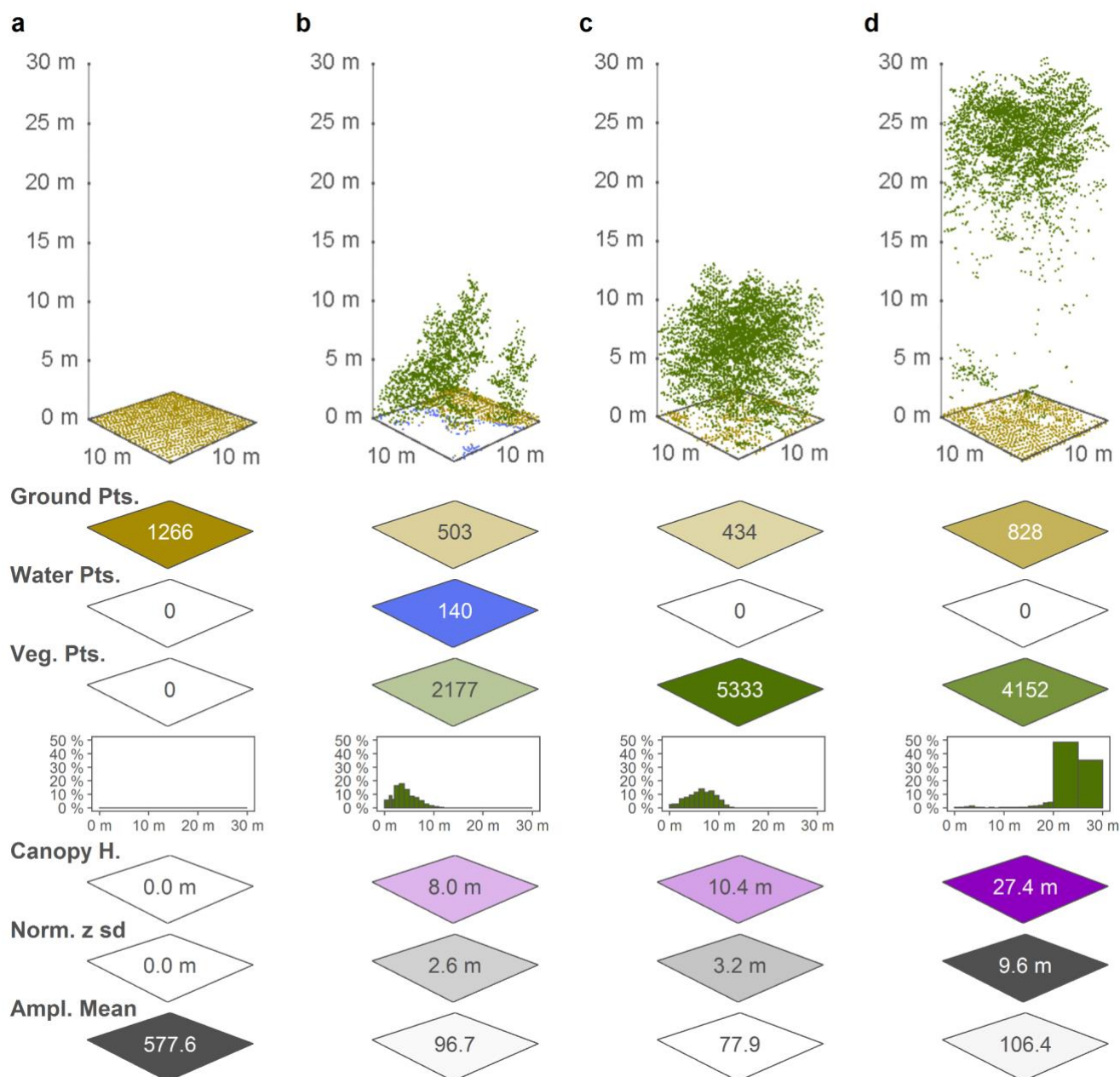
306 The TWI variable calculated for EcoDes-DK15 is subject to two main limitations: edge effects and small catchment size. Tiles  
307 with incomplete neighbourhoods (i.e., less than 8 direct neighbours are available) will suffer from edge effects in the direct  
308 vicinity of the relevant border and overall due to a reduced catchment size. Furthermore, even in the ideal case of the  
309 neighbourhood being complete, for most cells flow accumulation is therefore only calculated for the direct neighbourhood of  
310 a focal tile, comprising a 3 km x 3 km catchment area. While we hypothesize that, due to the relatively low variation in  
311 topography in Denmark, the TWI based on this comparably small catchment area will serve as a reasonable proxy for terrain-  
312 based wetness in most cases, it may be less reliable in areas with exceptionally high variation in topography or for lakes and  
313 rivers with large catchments. In addition, we would like to point the reader towards the general limitations of the TWI as a



314 proxy for soil moisture or terrain wetness as for example discussed by Kopecký et al. (2020). These general limitations should  
315 be taken into account when interpreting the TWI values provided in EcoDes-DK15.

### 316 **3.5 Point-cloud derived variables**

317 The DHM/Point-cloud point cloud was pre-classified into eleven point categories (Geodatastyrelsen, 2015). For the EcoDes-  
318 DK15 data set, we restricted the analysis to four of these classes, including ground points (“Terræn”) - class 2, water points  
319 (“Vand”) - class 9, as well as low (“lav”) , medium (“mellemhøj”) and high vegetation (“høj vegetation”) - classes 3, 4 and 5,  
320 respectively. We grouped the three vegetation classes into one single vegetation class and, instead of the pre-assigned height  
321 categories, considered a more detailed set of height bins (see point count and proportion descriptions below). We included all  
322 returns, i.e., first returns and echoes, in our analysis. All point cloud processing was carried out using OPALS and the OPALS  
323 Python bindings. As none of the point cloud derived variables required mosaicking to prevent edge-effects, we processed all  
324 point cloud variables on the focal tile only. After the initial ingestion of the LAZ-file for a tile into the OPALS data manager  
325 format (odm), we used the *OpalsAddInfo* module to add a normalised height (z) attribute to the points. For this attribute we  
326 subtracted the height of the ground derived from the corresponding DHM/Terrain raster (0.4 m grid size) from the height above  
327 sea level of each point. Figure 3 illustrates how the point cloud data translates to some of the variable outputs for four exemplary  
328 10 m x 10 m cells from the data set, and an overview of the point cloud derived variables for a 1 km x 1 km tile in Vejle Fjord  
329 in central Jutland is provided in Fig. 4.

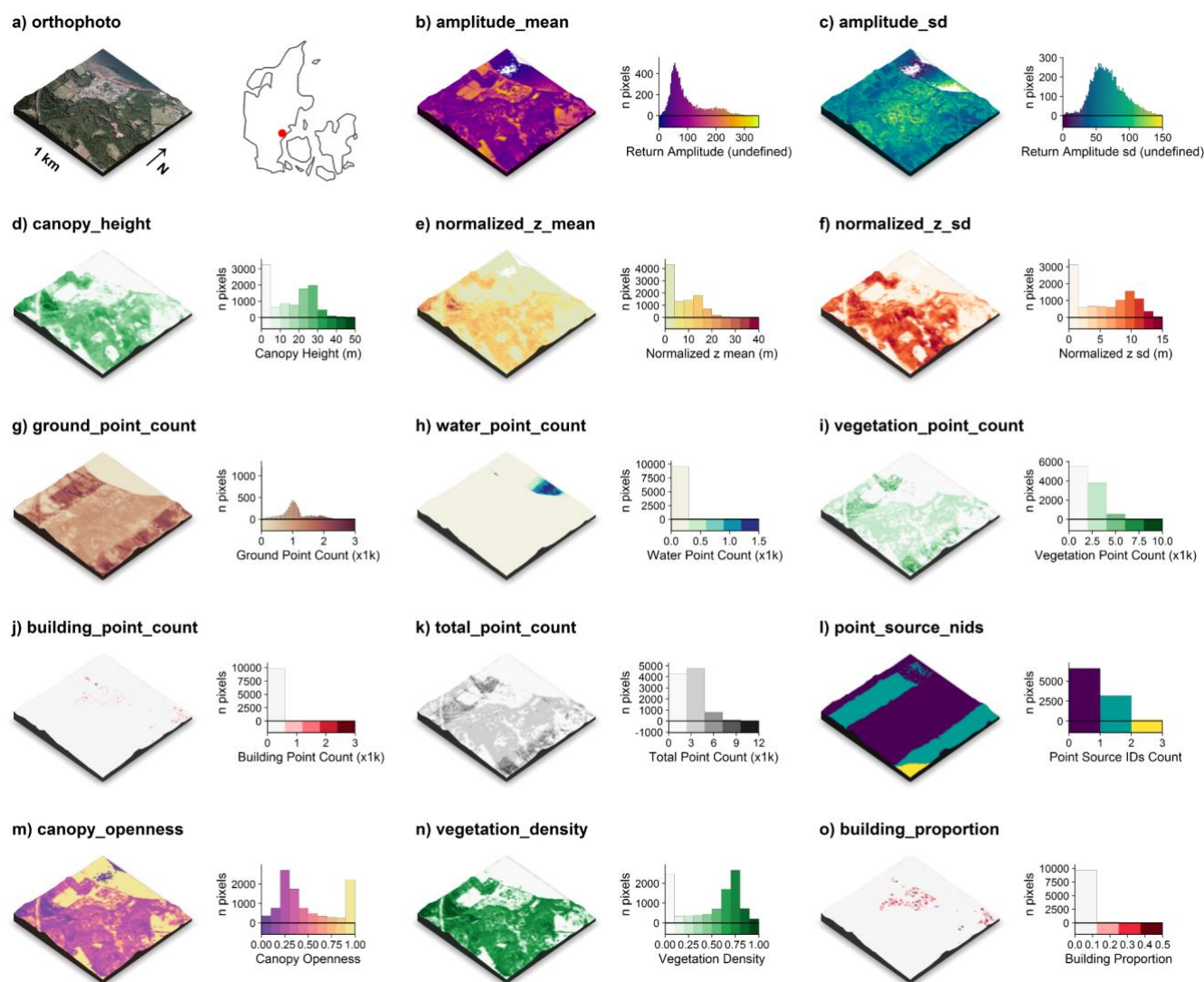


330

331 **Figure 3:** Point cloud examples for four 10 m x 10 m pixels and a selection of the associated EcoDes-DK15 variables derived  
 332 from the point clouds, illustrating the ecological meaning and some of the limitations of the EcoDes-DK15 data set. The 10 m  
 333 x 10 m pixels represent the following environments: a) an agricultural field, b) the edge of a forest / parkland pond with low  
 334 vegetation, c) a young plantation of dense coniferous trees, and d) old growth mixed-woodland. The EcoDes-DK15 variables  
 335 shown include (from the top) the total point counts for each pixel in the three main EcoDes-DK15 categories: 1) the number  
 336 of returns classified as ground, 2) the number of returns classified as water and 3) the number of returns classified as vegetation.



337 In addition, the relative proportion of vegetation points per predefined height bin is illustrated below the total vegetation point  
 338 count. Finally, the bottom three panels show the estimated canopy height (altitude above ground for the 95%-percentile of all  
 339 vegetation returns), the normalized z standard deviation (variation in height above ground for all return classes), and the mean  
 340 return amplitude for each cell.  
 341



342  
 343 **Figure 4:** Illustration of the point cloud derived variables for a 1 km x 1 km tile along Vejle Fjord (tile id: 6171\_541). An  
 344 orthophoto and the tile location relative to Denmark are shown in (a). The point cloud derived variables comprise of: c) the  
 345 mean return amplitude, d) the standard deviation in the return amplitude, e) the canopy height (vegetation returns only), f) the  
 346 mean of the normalized height above ground (all returns), g) the mean of the normalized height (all returns), h) the ground





347 point count, i) the water point count, j) the building point count, k) the total point count, l) the number of point sources (flight  
348 strips), m) the canopy openness, n) the vegetation density and o) the building proportion. For visualisation purposes, we  
349 amplified the altitude above sea-level by a factor of two in the 3D visualisations and divided the point counts by 1000. The 3D  
350 raster visualisations were generated using the rayshader v0.19.2 package in R (Morgan-Wall, 2020). Orthophotograph provided  
351 by the Danish Agency for Data Supply and Efficiency (<https://sdfe.dk/hent-data/fotos-og-geodanmark-data/>).

### 352 **3.5.1 Amplitude – mean and standard deviation (amplitude\_mean and amplitude\_sd)**

353 The amplitude attribute of a point in the DHM/Point-cloud is the actual amplitude of the return echoes, i.e., it describes the  
354 strength of the LiDAR return signals detected by the sensor. The variable is difficult to interpret in terms of its ecological  
355 meaning. Nonetheless, we believe that it is still useful for vegetation classifications, biodiversity analysis and other applications  
356 that perform well with proxy data. We calculate the arithmetic mean and standard deviation of the amplitude for all points  
357 within a 10 m x 10 m cell. Here, ‘all points’ refers to all points classified as ground, water, building, and vegetation points.  
358 Calculations were carried using the *OPALS Cell* module and results were stored as 32-bit floats. The amplitude attributes in  
359 the DHM/Point-cloud point clouds are not directly comparable when points originate from different point sources (e.g., flight  
360 strips), as the amplitude has not been calibrated and hence is sensitive to differences in sensor, sensor configuration and signal  
361 processing. Calculating summary metrics such as mean and standard deviation for a 10 m x 10 m cell where points from  
362 different point sources are present introduces additional complexities. In some cases, a 10 m cell might contain points from up  
363 to four different sources. We therefore recommend using the two amplitude variables with care, and - if possible - in  
364 conjunction with information on the point source ids contained in the *point\_source\_info* variables described below.

### 365 **3.5.3 Canopy height (canopy\_height)**

366 Canopy height is a key parameter of vegetation structure related to biomass and ecosystem functioning. We derived the canopy  
367 height in metres as the 95th-percentile of the normalised height above ground of all vegetation points within each 10 m x 10  
368 m cell using the *OPALS Cell* module. The resulting canopy heights were multiplied by a factor of 100, rounded to the nearest  
369 integer and stored as 16-bit integers. In cases where there were no vegetation points in any given cell, we set the canopy height  
370 value of the cell to zero metres. Please note that the canopy height is therefore also set as zero metres even if there are no points  
371 present in the cell at all (such as ground or water points). Furthermore, our algorithm calculates the canopy height even if there  
372 is only a small amount of vegetation points in a cell. In rare cases, this might lead to erroneous canopy-height readings if  
373 vegetation is found on artificial structures or points have been mis-classified. For example: A tall communications tower can  
374 be found just south of Aarhus and on top of this tower small patches of vegetation resulted in point returns being pre-classified  
375 as vegetation. The resulting canopy height for this cell is calculated as > 100 m above ground, which would not make sense if  
376 interpreted as a height of the vegetation above ground. For such cases, the building proportion variable may be used to separate  
377 cells with artificial structure from those with vegetation only. See also the “normalized\_z” variable below for a closely related  
378 measure.



379 **3.6.4 Normalised height - mean and standard deviation (normalized\_z\_mean and normalized\_z\_sd)**

380 Similar to the canopy height variable, the normalised height describes the structure properties of the point cloud above ground.  
381 The key difference between the two variables is that for the normalised height we also included non-vegetation points  
382 (buildings & ground) and derived the summary statistic as the mean rather than the 95%-quantile. For the normalised height  
383 variable, we also provide a measure of variation in form of the standard deviation. Specifically, we calculated the normalised  
384 mean and the standard deviation of the mean height above ground (normalised z attribute) for all points in each 10 m x 10 m  
385 grid cell using the *OPALS Cell* module. The results were multiplied by 100, rounded to the nearest integer and stored as 16-  
386 bit integers. We used the normalised z attribute generated during the ingestion of the point cloud reflecting the height of a  
387 point relative to the ground level determined by the DHM/Terrain raster. Here, all points refer to all points belonging either to  
388 the ground, water, building or vegetation class. By definition the normalised height mean will be highly correlated with the  
389 “canopy\_height” variable for cells where mainly vegetation points are present. We kept the American spelling of the variable  
390 name for legacy reasons with previous versions of the data set.

391 **3.6.5 Point counts (xxx\_point\_count\_xxx)**

392 The point count variables are intermediate variables used to generate the proportion variables described below. However, they  
393 can also be used to calculate tailored proportion variables relevant to addressing a specific ecological objective (see use-case  
394 example in Sect. 4.2). For EcoDes-DK15 we derived thirty point count variables for each 10 m x 10 m cells based on filtering  
395 of the pre-defined point classifications and separation by height above ground (normalised z) using the *OPALS Cell* module.  
396 All point counts were stored as 16-bit integers. These thirty variables contain six general point counts, including ground, water,  
397 vegetation, building and total point counts (Table 3), as well as twenty-four vegetation point counts separated in height bins  
398 (Table 4). Note that the number of returns within a 10 m cell is influenced by a) the number of point sources present in the  
399 cell, b) the relative position and distance of a cell to the point source when the data was collected (i.e., to the flight path), and  
400 c) by the point source themselves (i.e., differences between the LiDAR sensors deployed). The absolute counts are therefore  
401 not directly comparable between cells and need to be standardised first, for example by division of the total number of point  
402 counts as done for the point proportion variables derived by us.

403  
404 **Table 3:** General point count variables, as well as the height ranges and point classes included in each variable.  
405

Variable name	Height range	Point classes
ground_point_count_-01m-01m	-1 m to 1 m	ground points (class 2)
water_point_count_-01m-01m	-1 m to 1 m	water points (class 9)
ground_and_water_point_count_-01m-01m	-1 m to 1 m	ground and water points (classes 2,9)
vegetation_point_count_00m-50m	0 m to 50 m	vegetation points (classes 3,4,5)



building_point_count_-01m-50m	-1 m to 50 m	building points (class 6)
total_point_count_-01m-50m	-1 m to 50 m	ground, water, vegetation and building points (classes 2,3,4,5,6,9)

406  
 407  
 408  
 409

**Table 4:** Vegetation point count variables divided into twenty-four height bins. All vegetation point counts include the point classes 3,4 and 5.

Variable name	Height range
vegetation_point_count_00.0m-00.5m	0.0 m to 0.5 m
vegetation_point_count_00.5m-01.0m	0.5 m to 1.0 m
vegetation_point_count_01.0m-01.5m	1.0 m to 1.5 m
vegetation_point_count_01.5m-02.0m	1.5 m to 2.0 m
vegetation_point_count_02m-03m	2 m to 3 m
vegetation_point_count_03m-04m	3 m to 4 m
vegetation_point_count_04m-05m	4 m to 5 m
vegetation_point_count_05m-06m	5 m to 6 m
vegetation_point_count_06m-07m	6 m to 7 m
vegetation_point_count_07m-08m	7 m to 8 m
vegetation_point_count_08m-09m	8 m to 9 m
vegetation_point_count_09m-10m	9 m to 10 m
vegetation_point_count_10m-11m	10 m to 11 m
vegetation_point_count_11m-12m	11 m to 12 m
vegetation_point_count_12m-13m	12 m to 13 m
vegetation_point_count_13m-14m	13 m to 14 m
vegetation_point_count_14m-15m	14 m to 14 m
vegetation_point_count_15m-16m	15 m to 16 m
vegetation_point_count_16m-17m	16 m to 17 m
vegetation_point_count_17m-18m	17 m to 18 m
vegetation_point_count_18m-19m	18 m to 19 m
vegetation_point_count_19m-20m	19 m to 20 m
vegetation_point_count_20m-25m	20 m to 25 m



vegetation\_point\_count\_25m-50m                      25 m to 50 m

---

410 **3.6.6 Vegetation proportions by height bin (vegetation\_proportion\_XXX)**

411 The vegetation proportions by height bin are amongst the key parameters in the EcoDes-DK15 data set describing vegetation  
412 structure as they provide an indication of how the vegetation is distributed vertically within each cell of the raster. We  
413 calculated the proportions by dividing the vegetation count for each height bin (Table 4) by the total point count  
414 (total\_point\_count\_-01m-50m) within a given 10 m x 10 m cell. Resulting proportions were multiplied by a factor of 10000,  
415 rounded to the nearest integer and converted to 16-bit integers. All calculations were done using *gdal\_calc* based on the  
416 respective point count rasters (Sect. 3.3.5). The naming convention of the vegetation proportion variables  
417 “vegetation\_proportion\_XXX” follows the same convention as the vegetation point count variables (Table 4), whereby the suffix  
418 “XXX” is replaced with the respective height bin. Please note that height bins are spaced at 0.5 m intervals below 2 m and at 1  
419 m intervals between 2 m and 20 m. Furthermore, the range above 20 m is split into only 2 bins: 20 m to 25 m and 25 m to 50  
420 m.

421  
422 Given the properties of the DHM/Point-cloud we recommend being cautious when interpreting differences in the lower height  
423 bins. It is likely that the inaccuracies in the point cloud complicate clear separation between points less than half a metre apart.  
424 Furthermore, note that the proportions in the 0 m - 0.5 m bin are likely biased towards an underrepresentation of the vegetation  
425 proportion in this height bin, due to challenges in separating vegetation from ground points during the pre-classification. Lastly,  
426 keep in mind that dense canopy layers in the upper story of the canopy will reduce penetration of the light beam to the lower  
427 canopy layers. This may result in few returns in the lower layers (for example Fig 3 d) even though perhaps vegetation is  
428 present in those layers.

429 **3.6.7 Vegetation density or total vegetation proportion (vegetation\_density)**

430 Vegetation density is an important component of ecosystem structure. Here, we calculated the vegetation density as the ratio  
431 between the vegetation returns across all vertical height bins (vegetation\_point\_count\_00m-50m) and the total point count  
432 (total\_point\_count\_-01m-50m). Calculations were done using *gdal\_calc* based on the two point count rasters (Sect. 3.3.5).  
433 Results were multiplied by 10000, rounded to the nearest integer and stored as 16-bit integers. In addition to actual difference  
434 between vegetation density in a cell, the vegetation\_density variable is also influenced by the canopy properties such as the  
435 structure (dense upper layers will prevent penetration of the light beam to lower layers or even the ground) and texture  
436 (different canopies scatter light differently, causing lower or higher number of returns) and the points sources within a cell  
437 (e.g. multiple sources from different viewing angles provide a more complete estimate of the vegetation density). These  
438 additional influences are important to keep in mind when interpreting the vegetation\_density variable.



### 439 **3.6.7 Canopy openness, or ground and water proportion (canopy\_openness)**

440 Canopy openness is an important ecological descriptor particularly of forest canopies, as it describes the amount of light  
441 penetrating through to the levels of the canopy. To some degree the canopy openness serves as the inverse for the vegetation  
442 density. For EcoDes-DK15, we calculated the canopy openness of a 10 m x 10 m cell as the proportion of the ground and water  
443 points (ground\_and\_water\_point\_count\_-01m-01m) to the total point count (total\_point\_count\_-01m-50m) within the cell.  
444 The raster calculations were done using *gdal\_calc*. Results were multiplied by 10000, rounded to the nearest integer and stored  
445 as 16-bit integers. Please note that the same considerations as for the vegetation\_density variable (Sect. 3.3.7) regarding canopy  
446 properties and differences in point sources between the cells apply when interpreting the canopy\_openness variable. In  
447 addition, it is important to note that building points will reduce the canopy openness the same way that vegetation points  
448 would.

### 449 **3.6.8 Building proportion (building\_proportion)**

450 In a densely populated country such as Denmark, buildings form an important part of the landscape. For ecological studies the  
451 distance to the nearest buildings, their presence, absence or density may be of relevance. The building\_proportion variable of  
452 EcoDes-DK15 provides a proxy for how much building infrastructure can be found within a 10 m cell. We calculated the  
453 variable as the number of building points (building\_point\_count\_-01m-50m) divided by the total number of points  
454 (total\_point\_count\_-01m-50m) within each cell using *gdal\_calc*. Results were multiplied by 10000, rounded to the nearest  
455 integer and stored as 16-bit integers. While most returns from three dimensional infrastructure are classified as buildings in  
456 the DHM/Point-cloud, we would like to highlight that many roads are classified as ground (class 2) and some structures such  
457 as pylons and power lines were assigned a separate class (not described in (Geodatastyrelsen, 2015)). These structures are  
458 therefore not included in the building\_proportion variable. Finally, we would like to point the reader to the “DCE Basemap”  
459 (Levin, 2019) which may assist in the identification of basic land cover types that include buildings and other manmade  
460 structures.

## 461 **3.7 Auxiliary data**

462 In addition to the terrain and point cloud derived variables we provide three sets of auxiliary data with EcoDes-DK15. These  
463 are four layers of ALS point source information, a mask for inland water and a sea mask, as well as a shapefile of the footprints  
464 of the 1 km x 1 km tiles in the data set and their unique identifier.

### 465 **3.7.1 Point source information**

466 The point source attribute of the DHM/Point-cloud represents differences between sensor units or aircrafts that may have been  
467 used during the nationwide LiDAR campaign, differences in the acquisition time and date and differences in the viewpoint or  
468 acquisition angle of the cells. To aid in interpretation of variables that may be particularly influenced by point source, like the



469 amplitude variables or the vegetation proportions, we provide summary information about the point sources within each 10 m  
470 x 10 m cell. We summarised this information in four descriptor variables, the “point\_source\_counts”, “point\_source\_ids”,  
471 “point\_source\_nids” and “point\_source\_proportions”. For each tile (file name suffix = tile id), these variables are found in  
472 four subfolders bundled up in the parent “point\_source\_info” folder.

473 **point\_source\_ids** - Multi-layer raster containing one 16-bit integer layer for each point source id found in a tile. If a point  
474 with a given point source id is present the value of the cell is set to the point source id (an integer number) in the respective  
475 layer for the point source id, otherwise the value of a cell is set to 0. This multilayer raster can be used to match the file names  
476 of the point\_source\_counts and point\_source\_proportions rasters to a given point source id. Point source ids were extracted  
477 using *Opals Cell*.

478 **point\_source\_nids** - Single layer GeoTiff files containing the number of different point source ids in each cell stored as 16-  
479 bit integers. We calculated the number of point source ids based on the point\_source\_ids variable using *gdal\_calc*.

480 **point\_source\_counts** - For each tile there are multiple rasters (up to four), one raster for each point source id found in the  
481 point cloud of the tile (see the *point\_source\_ids* variable). These rasters are named with an additional suffix, which matches  
482 the integer point source id for which the point counts are given in the raster (e.g. point\_source\_counts\_xxxx\_xxx\_y\*, where  
483 xxxx\_xxx is the tile id and y\* the integer point source id). The rasters contain the number of points per 10 m x 10 m cell for  
484 the respective point source id in the tile. Counts were extracted using the *OPALS Cell* module and stored as 16-bit integers.

485 **point\_source\_proportions** - For each tile there are multiple rasters (up to four), one raster for each point source id found in  
486 the point cloud of the tile (see the *point\_source\_ids* variable). These rasters are named with an additional suffix, which matches  
487 the integer point source id for which the point proportions are given in the raster (e.g. point\_source\_proportions\_xxxx\_xxx\_y\*,  
488 where xxxx\_xxx is the tile id and y\* the integer point source id).. Each raster contains the proportion of the point counts for a  
489 given point source id in relation to the total point count per 10 m x 10 m cell. Calculations were carried out using *gdal\_calc*.  
490 The final proportions were multiplied by a factor of 10000, rounded to the nearest integer and stored as 16-bit integers.

### 491 **3.7.2 Water masks (inland\_water\_mask and sea\_mask)**

492 We also provide rasterized water masks for use cases in which require masking inland water bodies or the sea. To represent  
493 all permanent lakes in Denmark, we merged three shapefiles containing (1) lakes protected by the Danish nature protection  
494 legislation (§3, available at <https://arealinformation.miljoportal.dk>), (2) other valuable lakes (available on request at the  
495 Danish Farming Agency in the “good farming and environmental condition” data set) and (3) a layer containing the remaining  
496 rather small lakes and ponds (GeoDanmark, <https://kortforsyningen.dk/>). The combined shapefile is provided on the GitHub  
497 code repository (see below). We then burned the geometries within the shapefile into the 10 m x 10 m grid using *gdal\_rasterize*.  
498 The masks are binary, a cell value of 1 indicates land and a value of -9999 (no data) indicates sea or inland water, respectively.



499 When using the masks please consider that the shape, presence and absence of water bodies and coastlines may fluctuate over  
500 time. We created the masks to present a snapshot of the water bodies as close as possible to the time point of the DHM/Point-  
501 cloud acquisition (spring 2014 - summer 2015), but inaccuracies may still arise. When combining the data with more recent  
502 observations, keep in mind that inland water bodies and coastlines may have changed since then. Finally, while we aimed to  
503 produce the inland water mask to be as comprehensive as possible, some small ponds and water bodies may have been missed.  
504 Note also that while some rivers are included in the sea mask, the inland water mask does not include rivers or streams. The  
505 masks can be found in the “masks” subfolder of the complete data set.

### 506 **3.7.3 Footprint file (tile\_footprints.shp)**

507 To assist data access and creation of data subsets, we have produced an ESRI shapefile containing the footprints of all 1 km x  
508 1 km tiles in the EcoDes-DK15 data set. The shapefile was generated based on the “dtm\_10m” rasters and the tile identifier of  
509 each footprint geometry is specified in the “tile\_id” attribute column.

## 510 **4. Data access and ecological use case example**

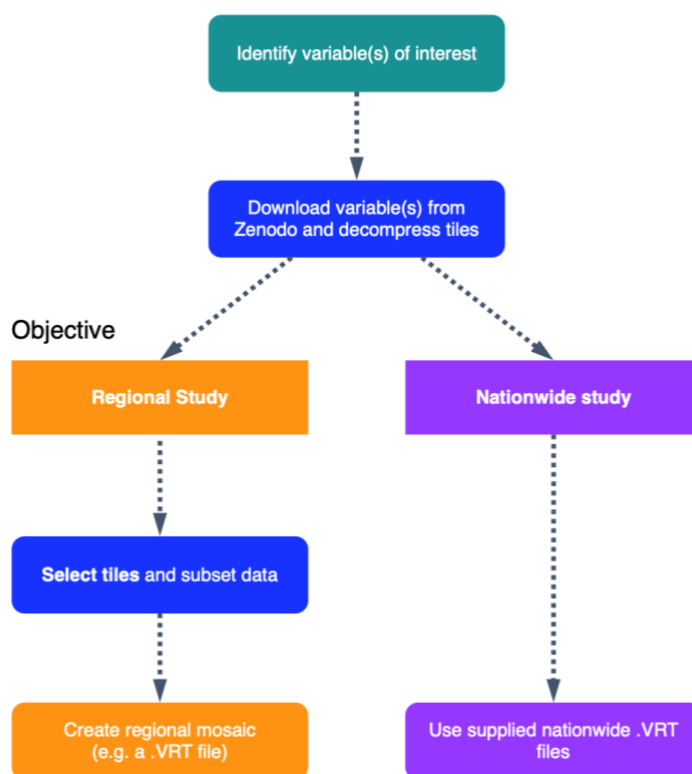
### 511 **4.1 Data access and handling**

512 Depending on the extent of the study, it may be preferable to work with a subset of the data set rather than the nationwide VRT  
513 files (Fig. 5). We suggest starting by identifying the relevant EcoDes-DK15 variables of interest, then retrieving the relevant  
514 data from the repository and decompressing the archives (instructions provided on data repository). If the study area of interest  
515 covers a large fraction of Denmark's extent and sufficient processing power is available, the nationwide VRT data should  
516 provide the most convenient access to the selected variables. However, if the study area does not cover a large proportion of  
517 Denmark, then we suggest sub setting the data using the tile footprints to decrease demands on computational resources. After  
518 sub setting, local / regional VRT files or mosaics can be generated if needed. We provide an example R script illustrating how  
519 this sub setting could be done for the use case example shown in the next section on the code repository  
520 ([manuscript/figure 6/subset data set.R](#)). We have also made the resulting subset available as a “teaser” (5 MB) to help the  
521 reader assess the value of EcoDes-DK15 without having to commit to the multi-gigabyte download of the complete data set  
522 (see Sect. 6).

523



## Data access



524

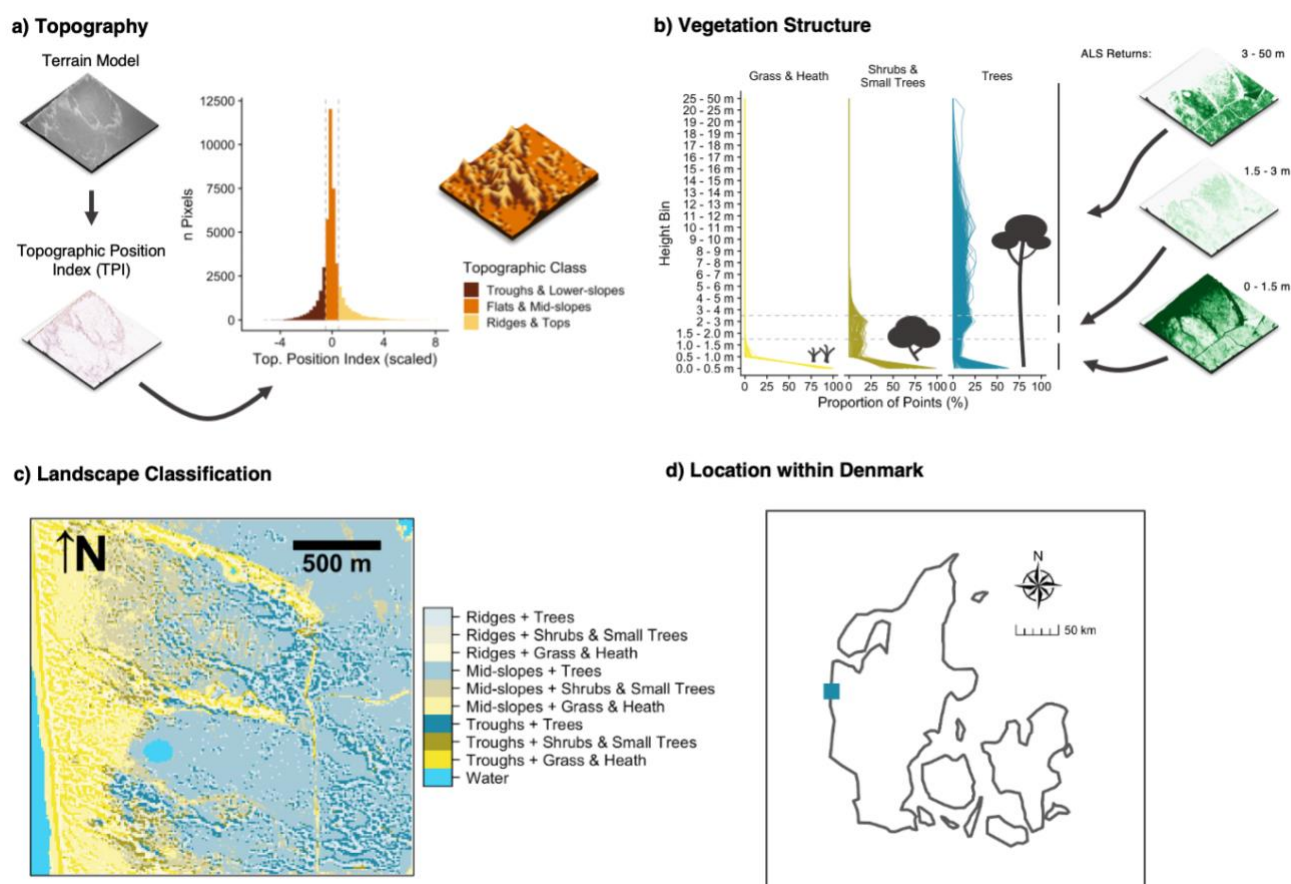
525 **Figure 5:** Schematic chart of two possible approaches for accessing and integrating EcoDes-DK15 data into ecological studies.  
526 The first step is to identify which variables are of interest, these variables can then be downloaded from the Zenodo repository  
527 and decompressed. Next a decision needs to be made whether the whole data set (nationwide) or only a subset of the tiles is  
528 required (e.g., a regional study). As the whole data set is relatively large (~ 87 GB), storage and processing limitations need to  
529 be taken into account when planning data processing and handling. If a subset of tiles is sufficient for a study, the provided  
530 tile footprints can be used to identify which tiles are required based on a geometry (e.g., a shapefile) of the study region(s).  
531 Finally, for easy data handling in subsequent analysis, a mosaic of the selected tiles can be created. For nationwide use we  
532 provided virtual mosaics (VRT files) containing all tiles for the variables. An R script illustrating how the sub setting can be  
533 done for a regional study can be found on the GitHub repository: [https://github.com/jakobjassmann/ecodes-dk-](https://github.com/jakobjassmann/ecodes-dk-lidar/blob/master/manuscript/figure_6/subset_dataset.R)  
534 [lidar/blob/master/manuscript/figure\\_6/subset\\_dataset.R](https://github.com/jakobjassmann/ecodes-dk-lidar/blob/master/manuscript/figure_6/subset_dataset.R).





535 **4.2 Use case example - ecological landscape stratification of Husby Klit nature protected area**

536 Figure 6 illustrates a use case for the EcoDes-DK15 data set with an example of an ecologically motivated landscape  
 537 stratification of the “Husby Klit” old-dune protected area in western Denmark. We developed this stratification for a group of  
 538 Master’s projects carrying out vegetation monitoring in the area. Our aim was to capture the variation in the dominant  
 539 vegetation based on vegetation structure as well as the variation in fine-scale topography created by the dune systems across  
 540 the landscape. In addition to using the variables already provided, the stratification required us to derive a topographic position  
 541 index as well as grouping the point densities in height bins relevant to the characteristics of the three most common dominant  
 542 vegetation types (grass and heath, *Pinus mugo* Turra, *Pinus sylvestris* L.) in the area. The source code for this figure contained  
 543 in the code repository provides an example of how this can be achieved ([manuscript/figure\\_6/figure\\_6.R](#)).  
 544



545  
 546 **Figure 6:** Use-case example: Landscape stratification of the Husby Klit protected area based on EcoDes-DK15 derived terrain  
 547 and vegetation structure descriptors. The target was to stratify the landscape of the Husby Klit “dune plantation” area in the  
 548 west of Denmark (56.2837 - 56.3024 °N, 8.1239 - 8.1600 °E) to facilitate stratified random sampling for vegetation monitoring.



549 We identified the four tiles overlapping with the boundaries of the protected area and derived a stratification based on two  
550 components: topographic position (a) and vegetation structure (b). We hypothesized that both components would influence  
551 the vegetation communities present. For the topographic position (a), we first derived and standardised the topographic position  
552 index (TPI) (Weiss, 2001) from the terrain model (dtm\_10m). Following (Weiss, 2001) we then classified each cell based on  
553 the scaled TPI into three categories. A scaled TPI below a value of -0.5 was classified as a “trough or lower-slope”, a scaled  
554 TPI between -0.5 and 0.5 as “mid-slope or flat”, and a scaled TPI above 0.5 as a “ridge or top”. For the vegetation structure  
555 component (b), we calculated the proportion of returns in three simplified height bins: 1) 0 m to 1.5 m, 2) 1.5 m to 3.0 m and  
556 3) 3.0 m - 50 m. Here we included both ground and vegetation returns as the divisor for the standardisation, but not the returns  
557 from buildings or water. Based on *a priori* knowledge we deduced that there are three dominant vegetation communities within  
558 the protected area: communities dominated by grass and heath with vegetation growth generally below 1.5 m, communities  
559 dominated by shrubs and small trees (including the invasive *Pinus mugo*) with vegetation growth predominantly below 3.0 m,  
560 and communities dominated by trees (including the native *Pinus sylvestris*), generally with growth above 3.0 m. We used this  
561 knowledge to assign the three vegetation classes based on the proportion of point returns in the simplified height bins. For the  
562 “grass and heath” class we used a strict cut off with no points present above 1.5 m. For the “shrubs and small trees” class we  
563 used a fuzzy cut off allowing the proportion of points in the 3.0 m and above bin to reach up to 10% of the maximum proportion  
564 found in this height bin. All remaining cells were then assigned to the “trees” class. Finally, we combined the two classifications  
565 into one as illustrated in c). Panel d) shows the location of the protected area within Denmark. The 3D raster visualisations  
566 were generated using the rayshader v0.19.2 package in R (Morgan-Wall, 2020).

## 567 **5. Discussion - limitations and future perspectives**

568 Our data set demonstrates how the complex information in ALS point cloud data sets spanning more than 40.000 km<sup>2</sup>, can be  
569 condensed into a compact data set of rasterized variables of interest for ecological studies. For the whole of Denmark, we  
570 provide 70 raster layers representing eighteen measures that describe a snapshot of vegetation height, structure and density, as  
571 well as topography and topography-derived habitat characteristics, including slope, aspect, solar radiation and wetness for the  
572 time period 2014-2015. These measures are of direct relevance for ecological research on species’ habitat characteristics,  
573 distribution modelling, biodiversity and conservation applications. Condensing the ALS derived information into a compact  
574 set of raster variables makes it more accessible to the community of ecological researchers and practitioners, allowing them to  
575 access information on the vertical structure of vegetation and terrain otherwise difficult to obtain for large extents such as those  
576 of a whole country.

577  
578 We would like to highlight some key ecological and physical limitations that should be kept in mind when using the data or  
579 derivatives. The EcoDes data set is a snapshot in time representing the collection period of approximately one and a half years  
580 between spring 2014 and summer 2015. Like anywhere on Earth, the landscapes of Denmark may change over time and by



581 the time point of publication of this data set over 5 years may have passed since the collection of the source data. External data  
582 sources containing information about on-going or past changes (such as satellite imagery - see below) might help overcome  
583 this bias. Additionally, the geographical differences in the timing of the point cloud collection across the country (Nord-Larsen  
584 et al., 2017), may introduce noise and could affect cross-comparability of the data between regions in some cases. Furthermore,  
585 there are implicit limitations in spatial scale due to the set grain size of the data set. We chose a 10 m x 10 m grid for efficiency  
586 in computation and data handling, as well as to overcome limitations in the density of the source point cloud (four to five  
587 points per m<sup>2</sup>). Our data set might therefore not serve well for capturing some ecological relevant variation in terrain and  
588 vegetation structures at scales below the 10 m x 10 m grain size. We believe that our data set is nonetheless valuable in  
589 providing ecologically relevant information at the geographical extent of Denmark.

590  
591 While some of the variables in the presented data set such as elevation, slope and vegetation height are quite straightforward  
592 to interpret, the ecological meaning of other variables – for example those related to vegetation structure – may not be as  
593 obvious as they are influenced by multiple ecological and sensing methodology related factors. The *amplitude*, *point count*  
594 and *point proportion* variables are amongst those measures. For example, while the (non-calibrated) amplitude in the  
595 DHM/Point-cloud source data may generally relate to the reflectance properties of the surface that generated the return, the  
596 incident light angle, scattering and subsequent generation of echoes may result in several different surfaces generating similar  
597 amplitude signatures. Furthermore, the point counts may be influenced by a whole suite of factors, including incident light  
598 angle, scattering, density of flight strips covering a given cell, as well as canopy properties - most importantly the penetration  
599 ability. While standardising the point counts as proportions to the total counts may help to account for some of these factors,  
600 it is likely that notable uncertainties will remain even in the proportions especially for lower layers of the canopy. Nonetheless,  
601 we believe that these measures can be informative if appropriate care is taken in their interpretation.

602 Two code developments could enhance the EcoDes-DK15 processing workflow in efficiency and transferability: using gdal  
603 Python bindings and switching to an open-source point cloud handler. First, for practical reasons we reverted to using gdal  
604 binaries rather than the Python bindings as we encountered issues with the gdal bindings provided by the OPALS shell on our  
605 computational server. Solving this issue and using the bindings instead of the binaries could reduce hard drive access time and  
606 overheads from launching subprocesses and therefore potentially speed up the raster manipulations in the workflow. However,  
607 as the point cloud processing takes the majority of time (we estimate 75-80%) we did not invest further resources to do so in  
608 the first development round. Secondly, while our Python source code is open source and freely available, OPALS itself requires  
609 the purchase of a software license, limiting the transferability of our code to projects which can afford the license. We did not  
610 explore alternatives to OPALS, but a redeveloped processing pipeline could make use of purely open source software  
611 benefiting from ongoing developments in the field, see for example the “Laserchicken” Python module (Meijer et al., 2020)  
612 and “lidR” R package (Roussel et al., 2020).

613



614 We believe that to realise the full potential of ALS derived data such as EcoDes-DK15 these data sets are ideally combined  
615 with other data sources including climate, field data and remote sensing observations. Climate data is especially relevant for  
616 addressing research on species-habitat relationships, distribution models and biodiversity studies and many studies have  
617 demonstrated the power of ALS observations in complementing climate data for such exercises (Coops et al., 2016; Zellweger  
618 et al., 2016). Like for other remote sensing products, field data is essential for validating inferences and putting biological  
619 meaning into ALS data (Coops et al., 2021) - this applies especially to the more complex structural vegetation measures in  
620 EcoDes-DK15. This could be achieved through field surveys combined with terrestrial and drone based ALS data, where the  
621 point density is much higher (e.g., Madsen et al., 2020). The potential benefits from fusing ALS data with other remote sensing  
622 products have been realised early on (Hyde et al., 2005) and demonstrated again since then (e.g., Coops et al., 2021;  
623 Montgomery et al., 2019; Manzanera et al., 2016). However, note that data fusion does not provide additional value in every  
624 use case (Xu et al., 2018; Ceballos et al., 2015; Boelman et al., 2016). We still believe that there is tremendous potential in  
625 combining EcoDes-DK15 with other types of remote sensing data. Fine-grain optical imagery could provide proxies for  
626 horizontal vegetation structure in grasslands where the vegetation is too small to be captured by the DHM/Point-cloud density  
627 (e.g., Malmstrom et al., 2017; Pazúr et al., 2021) and satellite derived time-series can provide unique temporal perspectives  
628 that describe parameters of seasonality (e.g., Boelman et al., 2016) and the historical context on disturbances and landcover  
629 change not captured in the single time-point ALS data (e.g., Senf et al., 2017; Pekel et al., 2016).

## 630 **6. Data availability**

631 The data is openly available under a Creative Commons by Attribution 4.0 license on Zenodo:

632 <https://doi.org/10.5281/zenodo.4756556> (Assmann et al., 2021)

633

634 A small example subset “teaser” (5 MB) covering the 9 km x 9 km of the Husby Klit area (Fig. 6) is available on the GitHub  
635 code repository:

636 [https://github.com/jakobjassmann/ecodes-dk-lidar/blob/master/manuscript/figure\\_6/EcoDes-DK15\\_teaser.zip](https://github.com/jakobjassmann/ecodes-dk-lidar/blob/master/manuscript/figure_6/EcoDes-DK15_teaser.zip)

637

## 638 **7. Code availability**

639 The source code for the processing pipeline is openly available under a simplified BSD license via GitHub:

640 <https://github.com/jakobjassmann/ecodes-dk-lidar>



## 641 **8. Conclusions**

642 Open data sets like EcoDes-DK15 will allow ecologists with limited computational resources and little expertise in handling  
643 LiDAR point clouds to use large-scale ALS data for their research. We see our efforts not only as a first step for providing  
644 ready-to-use descriptors of local vegetation and terrain features, but also for providing an example workflow and tools that  
645 allow for the replication of the processing. We have described and documented the measures of terrain and vegetation structure  
646 contained in the data set and pointed out possible applications and limitations. We are confident that EcoDes-DK15 provides  
647 a meaningful collection of ecological descriptors at a 10 x 10 m resolution for the extent of a whole country and we encourage  
648 the community to use our workflow and collection of codes as inspirations to process other large-scale ALS data sets in a  
649 similar manner. Ultimately, we hope the publication of this data set will help facilitate the uptake of ALS-derived information  
650 by ecological researchers and practitioners in Denmark and beyond.

## 651 **9. Author contributions**

652 All co-authors developed the data set with focus on its ecological relevance, providing input on the ecological meaning, spatial  
653 scale and calculation of the variables. JJA developed the code with input from JEM. JJA carried out the computations. JJA led  
654 the writing of the manuscript, with all co-authors contributing to the manuscript in a collaborative manner. SN provided  
655 funding and supervision for this project.

## 656 **10. Competing interests**

657 The authors declare that they have no conflict of interest.

## 658 **11. Acknowledgements**

659 We would like to thank Andràs Zlinszky for his contributions to earlier versions of the data set and Charles Davison for  
660 feedback regarding data use and handling. Funding for this work was provided by the Carlsberg Foundation (Distinguished  
661 Associate Professor Fellowships) and Aarhus University Research Foundation (AUFF-E-2015-FLS-8-73) to Signe Normand  
662 (SN). This work is a contribution to SustainScapes – Center for Sustainable Landscapes under Global Change (grant  
663 NNF200C0059595 to SN).

## 664 **12. References**

665 Assmann, J. J., Moeslund, J. E., Treier, U. A., and Normand, S.: EcoDes-DK15: High-resolution ecological descriptors of  
666 vegetation and terrain derived from Denmark's national airborne laser scanning data set, Zenodo [data set],  
667 <https://doi.org/10.5281/zenodo.4756556>, 2021.



- 668 Bakx, T. R. M., Koma, Z., Seijmonsbergen, A. C., and Kissling, W. D.: Use and categorization of Light Detection and Ranging  
669 vegetation metrics in avian diversity and species distribution research, *Divers Distrib*, 25, 1045–1059,  
670 <https://doi.org/10.1111/ddi.12915>, 2019.
- 671 Beven, K. J. and Kirkby, M. J.: A physically based, variable contributing area model of basin hydrology / Un modèle à base  
672 physique de zone d'appel variable de l'hydrologie du bassin versant, *Hyrdol Sci B*, 24, 43–69,  
673 <https://doi.org/10.1080/02626667909491834>, 1979.
- 674 Boelman, N. T., Holbrook, J. D., Greaves, H. E., Krause, J. S., Chmura, H. E., Magney, T. S., Perez, J. H., Eitel, J. U. H.,  
675 Gough, L., Vierling, K. T., Wingfield, J. C., and Vierling, L. A.: Airborne laser scanning and spectral remote sensing  
676 give a bird's eye perspective on arctic tundra breeding habitat at multiple spatial scales, *Remote Sens Environ*, 184,  
677 337–349, <https://doi.org/10.1016/j.rse.2016.07.012>, 2016.
- 678 Böhner, J. and Selige, T.: Spatial Prediction Of Soil Attributes Using Terrain Analysis And Climate Regionalisation, *Göttinger*  
679 *Geographische Abhandlungen*, 115, 13–120, 2006.
- 680 Ceballos, A., Hernández, J., Corvalán, P., and Galleguillos, M.: Comparison of Airborne LiDAR and Satellite Hyperspectral  
681 Remote Sensing to Estimate Vascular Plant Richness in Deciduous Mediterranean Forests of Central Chile, *Remote*  
682 *Sens-Basel*, 7, 2692–2714, <https://doi.org/10.3390/rs70302692>, 2015.
- 683 Conrad, O., Bechtel, B., Bock, M., Dietrich, H., Fischer, E., Gerlitz, L., Wehberg, J., Wichmann, V., and Böhner, J.: System  
684 for Automated Geoscientific Analyses (SAGA) v. 2.1.4, *Geosci Model Dev*, 8, 1991–2007,  
685 <https://doi.org/10.5194/gmd-8-1991-2015>, 2015.
- 686 Coops, N. C., Tompaski, P., Nijland, W., Rickbeil, G. J. M., Nielsen, S. E., Bater, C. W., and Stadt, J. J.: A forest structure  
687 habitat index based on airborne laser scanning data, *Ecol Indic*, 67, 346–357,  
688 <https://doi.org/10.1016/j.ecolind.2016.02.057>, 2016.
- 689 Coops, N. C., Tompaski, P., Goodbody, T. R. H., Queinnec, M., Luther, J. E., Bolton, D. K., White, J. C., Wulder, M. A., van  
690 Lier, O. R., and Hermosilla, T.: Modelling lidar-derived estimates of forest attributes over space and time: A review  
691 of approaches and future trends, *Remote Sens Environ*, 260, 112477, <https://doi.org/10.1016/j.rse.2021.112477>, 2021.
- 692 Freeman, T. G.: Calculating catchment area with divergent flow based on a regular grid, *Comput Geosci*, 17, 413–422,  
693 [https://doi.org/10.1016/0098-3004\(91\)90048-I](https://doi.org/10.1016/0098-3004(91)90048-I), 1991.
- 694 Froidevaux, J. S. P., Zellweger, F., Bollmann, K., Jones, G., and Obrist, M. K.: From field surveys to LiDAR: Shining a light  
695 on how bats respond to forest structure, *Remote Sens Environ*, 175, 242–250,  
696 <https://doi.org/10.1016/j.rse.2015.12.038>, 2016.
- 697 GDAL/OGR contributors: GDAL/OGR Geospatial Data Abstraction software Library, Open Source Geospatial Foundation,  
698 2018.
- 699 Geodatastyrelsen: Dataspecifikation for Danmarks Højdemodel Punktsky. Data version 2.0 - Januar 2015., Geodatastyrelsen,  
700 Copenhagen, 2015.
- 701 Gruber, S. and Peckahm, S.: Land-Surface Parameters and Objects in Hydrology, in: *Geomorphometry: Concepts, Software,*  
702 *Applications*, vol. 33, edited by: Hengl, T. and Reuter, H. I., Elsevier, 293–308, 2008.
- 703 Guo, X., Coops, N. C., Tompaski, P., Nielsen, S. E., Bater, C. W., and John Stadt, J.: Regional mapping of vegetation structure  
704 for biodiversity monitoring using airborne lidar data, *Ecol Inform*, 38, 50–61,  
705 <https://doi.org/10.1016/j.ecoinf.2017.01.005>, 2017.
- 706 Haralick, R. M.: Ridges and valleys on digital images, *Comput Vision Graph*, 22, 28–38, [https://doi.org/10.1016/0734-189X\(83\)90094-4](https://doi.org/10.1016/0734-189X(83)90094-4), 1983.
- 707
- 708 Horn, B. K. P.: Hill shading and the reflectance map, *P IEEE*, 69, 14–47, <https://doi.org/10.1109/PROC.1981.11918>, 1981.
- 709 Hyde, P., Dubayah, R., Peterson, B., Blair, J. B., Hofton, M., Hunsaker, C., Knox, R., and Walker, W.: Mapping forest structure  
710 for wildlife habitat analysis using waveform lidar: Validation of montane ecosystems, *Remote Sens Environ*, 96, 427–  
711 437, <https://doi.org/10.1016/j.rse.2005.03.005>, 2005.
- 712 IPBES: Global assessment report on biodiversity and ecosystem services of the Intergovernmental Science-Policy Platform on  
713 Biodiversity and Ecosystem Services., edited by: Brondizio, E. S., Díaz, S., and Settele, J., IPBES secretariat, Bonn,  
714 Germany., 2019.
- 715 Kopecký, M., Macek, M., and Wild, J.: Topographic Wetness Index calculation guidelines based on measured soil moisture  
716 and plant species composition, *Sci Total Environ*, 143785, <https://doi.org/10.1016/j.scitotenv.2020.143785>, 2020.



- 717 Leutner, B. F., Reineking, B., Müller, J., Bachmann, M., Beierkuhnlein, C., Dech, S., and Wegmann, M.: Modelling Forest  $\alpha$ -  
718 Diversity and Floristic Composition — On the Added Value of LiDAR plus Hyperspectral Remote Sensing, *Remote*  
719 *Sens-Basel*, 4, 2818–2845, <https://doi.org/10.3390/rs4092818>, 2012.
- 720 Levin, G.: Basemap03. Technical documentation of the method for elaboration of a land-use and land-cover map for Denmark,  
721 Aarhus University, DCE – Danish Centre for Environment and Energy, Aarhus, Denmark, 2019.
- 722 Lopatin, J., Dolos, K., Hernández, H. J., Galleguillos, M., and Fassnacht, F. E.: Comparing Generalized Linear Models and  
723 random forest to model vascular plant species richness using LiDAR data in a natural forest in central Chile, *Remote*  
724 *Sens Environ*, 173, 200–210, <https://doi.org/10.1016/j.rse.2015.11.029>, 2016.
- 725 Madsen, B., Treier, U. A., Zlinszky, A., Lucieer, A., and Normand, S.: Detecting shrub encroachment in seminatural grasslands  
726 using UAS LiDAR, *Ecol Evol*, 10, 4876–4902, <https://doi.org/10.1002/ece3.6240>, 2020.
- 727 Malmstrom, C. M., Butterfield, H. S., Planck, L., Long, C. W., and Eviner, V. T.: Novel fine-scale aerial mapping approach  
728 quantifies grassland weed cover dynamics and response to management, *PLOS ONE*, 12, e0181665,  
729 <https://doi.org/10.1371/journal.pone.0181665>, 2017.
- 730 Manzanera, J. A., García-Abril, A., Pascual, C., Tejera, R., Martín-Fernández, S., Tokola, T., and Valbuena, R.: Fusion of  
731 airborne LiDAR and multispectral sensors reveals synergic capabilities in forest structure characterization, *GISci*  
732 *Remote Sens*, 53, 723–738, <https://doi.org/10.1080/15481603.2016.1231605>, 2016.
- 733 Mao, L., Dennett, J., Bater, C. W., Tompalski, P., Coops, N. C., Farr, D., Kohler, M., White, B., Stadt, J. J., and Nielsen, S.  
734 E.: Using airborne laser scanning to predict plant species richness and assess conservation threats in the oil sands  
735 region of Alberta’s boreal forest, *Forest Ecol Manag*, 409, 29–37, <https://doi.org/10.1016/j.foreco.2017.11.017>, 2018.
- 736 McCune, B. and Keon, D.: Equations for potential annual direct incident radiation and heat load, *J Veg Sci*, 13, 603–606,  
737 <https://doi.org/10.1111/j.1654-1103.2002.tb02087.x>, 2002.
- 738 Meijer, C., Grootes, M. W., Koma, Z., Dzigan, Y., Gonçalves, R., Andela, B., van den Oord, G., Ranguelova, E., Renaud, N.,  
739 and Kissling, W. D.: Laserchicken—A tool for distributed feature calculation from massive LiDAR point cloud  
740 datasets, *SoftwareX*, 12, 100626, <https://doi.org/10.1016/j.softx.2020.100626>, 2020.
- 741 Moeslund, J. E., Arge, L., Bøcher, P. K., Dalgaard, T., Odgaard, M. V., Nygaard, B., and Svenning, J.-C.: Topographically  
742 controlled soil moisture is the primary driver of local vegetation patterns across a lowland region, *Ecosphere*, 4, art91,  
743 <https://doi.org/10.1890/ES13-00134.1>, 2013.
- 744 Moeslund, J. E., Zlinszky, A., Ejrnæs, R., Brunbjerg, A. K., Bøcher, P. K., Svenning, J.-C., and Normand, S.: Light detection  
745 and ranging explains diversity of plants, fungi, lichens, and bryophytes across multiple habitats and large geographic  
746 extent, *Ecol Appl*, 29, e01907, <https://doi.org/10.1002/eap.1907>, 2019.
- 747 Montgomery, J., Brisco, B., Chasmer, L., Devito, K., Cobbaert, D., and Hopkinson, C.: SAR and Lidar Temporal Data Fusion  
748 Approaches to Boreal Wetland Ecosystem Monitoring, *Remote Sens-Basel*, 11, 161,  
749 <https://doi.org/10.3390/rs11020161>, 2019.
- 750 Moore, I. D., Grayson, R. B., and Ladson, A. R.: Digital terrain modelling: A review of hydrological, geomorphological, and  
751 biological applications, *Hydrol Process*, 5, 3–30, <https://doi.org/10.1002/hyp.3360050103>, 1991.
- 752 Morgan-Wall, T.: rayshader: Create Maps and Visualize Data in 2D and 3D, 2020.
- 753 Nord-Larsen, T., Riis-Nielsen, T., and Ottosen, M. B.: Forest resource map of Denmark: Mapping of Danish forest resource  
754 using ALS from 2014-2015, Department of Geosciences and Natural Resource Management, University of  
755 Copenhagen, Copenhagen, Denmark, 2017.
- 756 Pazúr, R., Huber, N., Weber, D., Ginzler, C., and Price, B.: A national extent map of cropland and grassland for Switzerland  
757 based on Sentinel-2 data, *Earth Syst Sci Data*, 1–14, <https://doi.org/10.5194/essd-2021-60>, 2021.
- 758 Pekel, J.-F., Cottam, A., Gorelick, N., and Belward, A. S.: High-resolution mapping of global surface water and its long-term  
759 changes, 540, 418–422, <https://doi.org/10.1038/nature20584>, 2016.
- 760 Peura, M., Silveyra Gonzalez, R., Müller, J., Heurich, M., Vierling, L. A., Mönkkönen, M., and Bässler, C.: Mapping a ‘cryptic  
761 kingdom’: Performance of lidar derived environmental variables in modelling the occurrence of forest fungi, *Remote*  
762 *Sens Environ*, 186, 428–438, <https://doi.org/10.1016/j.rse.2016.09.003>, 2016.
- 763 Pfeifer, N., Mandlbürger, G., Otepka, J., and Karel, W.: OPALS – A framework for Airborne Laser Scanning data analysis,  
764 *Comput Environ Urban*, 45, 125–136, <https://doi.org/10.1016/j.compenvurbysys.2013.11.002>, 2014.
- 765 Quinn, P., Beven, K., Chevallier, P., and Planchon, O.: The prediction of hillslope flow paths for distributed hydrological  
766 modelling using digital terrain models, *Hydrol Process*, 5, 59–79, <https://doi.org/10.1002/hyp.3360050106>, 1991.



- 767 Reback, J., McKinney, W., Bossche, J. V. den, jbrockmendel, Augspurger, T., Cloud, P., gfyong, Sinhrks, Klein, A., Tratner,  
768 J., She, C., Roeschke, M., Petersen, T., Ayd, W., Hayden, A., Hawkins, S., Schendel, J., Garcia, M., Jancauskas, V.,  
769 Battiston, P., Seabold, S., chris-b1, h-vetinari, Hoyer, S., Overmeire, W., Mehyar, M., nouri, behzad, Kluyver, T.,  
770 Whelan, C., and Chen, K. W.: pandas-dev/pandas: v0.24.2, Zenodo, <https://doi.org/10.5281/zenodo.3509135>, 2019.
- 771 Roussel, J.-R., Auty, D., Coops, N. C., Tompalski, P., Goodbody, T. R. H., Meador, A. S., Bourdon, J.-F., de Boissieu, F., and  
772 Achim, A.: lidR: An R package for analysis of Airborne Laser Scanning (ALS) data, *Remote Sens Environ*, 251,  
773 112061, <https://doi.org/10.1016/j.rse.2020.112061>, 2020.
- 774 SAGA-GIS Tool Library Documentation v7.8.2: [http://www.saga-gis.org/saga\\_tool\\_doc/7.8.2/index.html](http://www.saga-gis.org/saga_tool_doc/7.8.2/index.html), last access: 28 June  
775 2021.
- 776 Senf, C., Pflugmacher, D., Hostert, P., and Seidl, R.: Using Landsat time series for characterizing forest disturbance dynamics  
777 in the coupled human and natural systems of Central Europe, *ISPRS J Photogramm*, 130, 453–463,  
778 <https://doi.org/10.1016/j.isprsjprs.2017.07.004>, 2017.
- 779 Thers, H., Brunbjerg, A. K., Læssøe, T., Ejrnæs, R., Bøcher, P. K., and Svenning, J.-C.: Lidar-derived variables as a proxy for  
780 fungal species richness and composition in temperate Northern Europe, *Remote Sens Environ*, 200, 102–113,  
781 <https://doi.org/10.1016/j.rse.2017.08.011>, 2017.
- 782 Tweedy, P. J., Moriarty, K. M., Bailey, J. D., and Epps, C. W.: Using fine scale resolution vegetation data from LiDAR and  
783 ground-based sampling to predict Pacific marten resting habitat at multiple spatial scales, *Forest Ecol Manag*, 452,  
784 117556, <https://doi.org/10.1016/j.foreco.2019.117556>, 2019.
- 785 Valbuena, R., O'Connor, B., Zellweger, F., Simonson, W., Vihervaara, P., Maltamo, M., Silva, C. A., Almeida, D. R. A.,  
786 Danks, F., Morsdorf, F., Chirici, G., Lucas, R., Coomes, D. A., and Coops, N. C.: Standardizing Ecosystem  
787 Morphological Traits from 3D Information Sources, *Trends Ecol Evol*, S0169534720300811,  
788 <https://doi.org/10.1016/j.tree.2020.03.006>, 2020.
- 789 Van Rossum, G. and Drake Jr, F. L.: Python reference manual, Centrum voor Wiskunde en Informatica Amsterdam, 1995.
- 790 Vierling, K. T., Vierling, L. A., Gould, W. A., Martinuzzi, S., and Clawges, R. M.: Lidar: shedding new light on habitat  
791 characterization and modeling, *Front Ecol Environ*, 6, 90–98, <https://doi.org/10.1890/070001>, 2008.
- 792 Vo, A.-V., Laefer, D. F., and Bertolotto, M.: Airborne laser scanning data storage and indexing: state-of-the-art review, *Int J*  
793 *Remote Sens*, 37, 6187–6204, <https://doi.org/10.1080/01431161.2016.1256511>, 2016.
- 794 Wagner, W., Ullrich, A., Ducic, V., Melzer, T., and Studnicka, N.: Gaussian decomposition and calibration of a novel small-  
795 footprint full-waveform digitising airborne laser scanner, *ISPRS J Photogramm*, 60, 100–112,  
796 <https://doi.org/10.1016/j.isprsjprs.2005.12.001>, 2006.
- 797 Wang, L. and Liu, H.: An efficient method for identifying and filling surface depressions in digital elevation models for  
798 hydrologic analysis and modelling, *Int J Geogr Inf Sci*, 20, 193–213, <https://doi.org/10.1080/13658810500433453>,  
799 2006.
- 800 Weiss, A.: Topographic position and landforms analysis, in: Poster presentation, ESRI user conference, San Diego, CA, 2001.
- 801 Xu, C., Manley, B., and Morgenroth, J.: Evaluation of modelling approaches in predicting forest volume and stand age for  
802 small-scale plantation forests in New Zealand with RapidEye and LiDAR, *Int J Appl Earth Obs*, 73, 386–396,  
803 <https://doi.org/10.1016/j.jag.2018.06.021>, 2018.
- 804 Yokoyama, R.: Visualizing Topography by Openness: A New Application of Image Processing to Digital Elevation Models,  
805 *Photogramm Eng Rem S*, 68, 257–265, 2002.
- 806 Zellweger, F., Baltensweiler, A., Ginzler, C., Roth, T., Braunisch, V., Bugmann, H., and Bollmann, K.: Environmental  
807 predictors of species richness in forest landscapes: abiotic factors versus vegetation structure, *J Biogeogr*, 43, 1080–  
808 1090, <https://doi.org/10.1111/jbi.12696>, 2016.
- 809